GEOMETRIC METHODS FOR MODELING AND CONTROL OF A FREE-SWIMMING CARANGIFORM FISH ROBOT

Kristi A. Morgansen*
Department of Aeronautics and Astronautics
University of Washington, Box 352400
Seattle, WA 98195-2400
morgansen@aa.washington.edu

Abstract

In this paper, we apply techniques from geometric mechanics and geometric nonlinear control theory to model and construct trajectory tracking algorithms for a free-swimming underwater vehicle that locomotes and maneuvers using a two-link actuated "tail" and actuated "pectoral fin" bowplanes. Restricting consideration of fluid forces to the simple effects of added mass and quasistatic lift and drag, the resulting system model can be expressed in a control-affine structure. With particular choices of oscillatory actuation of the four system joints, we can construct maneuvers such as swimming forward, turning in the plane, out of plane turns, surfacing, and diving. Using state error feedback, we then show how to stabilize turning and depth for such a vehicle. Results are demonstrated in simulation and in experiment using the University of Washington prototype robot fish.

1 Introduction

During the past several years, growing interest has developed in the area of design and control of underwater robots that propel and maneuver themselves with fins rather than with a propeller or thrusters. The study of underwater locomotion has long been a subject of interest to the biological community [6, 12, 17]. The robotics and engineering communities have recently been inspired by this research to construct biologically inspired mechanisms that mimic the behavior of individual and groups of swimming lifeforms. The motivation for this work comes from the high maneuverability, low drag and low hydrodynamic noise that fish demonstrate over conventional propeller-driven underwater vehicles.

Some of the most impressive swimmers in nature propel themselves by the *carangiform* style of swimming. In carangiform swimming, the front two-thirds of the fish's body moves in a largely rigid way, with the propulsive body movements being confined to the rear third of the body—primarily the tail. Carangiform movement is one of the easiest to replicate from a mechanical design perspective. Previous work in this area has come from the robopike and robotuna projects at MIT and Draper Laboratories [2, 3, 21] as well as work at the University of Minnesota [11, 18] and Caltech [8, 9, 13, 14, 15, 16]. These efforts have focused primarily on planar models of swimming–the robots are restricted to a plane perpendicular to gravity. Changes in depth have generally been achieved with active buoyancy control and gliding [4], or internal mass distribution [25]. The use of pectoral fins has received less attention but initial work with such actuators can be found in [7].

Prior robotic fish research has focused on the issue of propulsion efficiency and fluid flow effects and has been primarily empirical using techniques such as genetic algorithms and learning methods. The complexity of producing a high fidelity model of the interaction of an articulated mechanical system and a fluid environment has been prohibitive to developing dynamical systems methods for fish type propulsion. Our work differs from many of the earlier studies in one main respect: we focus on the issue of geometric methods for modeling, motion planning and control. The approach we will use here is based on a highly simplified quasi-static lift and drag model of the forces on the fish body and tail [13, 14]. Extensions of the ideas from these references and [15, 16] to a fully autonomous, untethered free swimming robot with both caudal and pectoral fins is the focus of the work in this paper.

While our quasi-static lift and drag model does not capture every detail of the fluid-body interaction, it does serve several useful purposes. First, it allows us to write a description of our system in a control affine form where the control inputs enter linearly. We can therefore apply known methods to analyze control performance. Importantly, we note that the linearized equations are not controllable, precluding the use of standard linear methods for trajectory tracking. However, this system is controllable in a limited nonlinear sense. As we will

*This material is based upon work supported in part by the NSF under Grant SBE-0123552 and in part by the NSF under Grant CMS-0238461.

show, application of recent results in nonlinear control theory demonstrate that we can generate a variety of gaits for this system. In particular, our approach predicts inputs that cause turning. These maneuvers would be difficult to find by intuition or by direct adoption of the maneuvers of real fish whose mechanical structure is sufficiently different than our robot fish. Second, it is not absolutely necessary to capture all fluid flow details for the purposes of control design, since control feedback can compensate for reasonable modeling errors. In fact, an important conclusion of our work is that the detailed computational or experimental models of fluid flow that have been developed in prior work [24] are not completely necessary for the purposes of robot fish control system design.

The paper is organized as follows. In Section 2, we discuss the construction and physical properties of our experimental fin-actuated robot. We then present a system model amenable to control theoretic methods as well as a simplified version in Section 3 for focus on the pectoral fins. Controllability and motion generation are discussed in 4. Control inputs to generate particular gaits are given in Section 5 and demonstrated in simulation. In Section 6 we present experimental results for the input functions derived in the previous sections. Finally, we discuss these results, present concluding remarks and directions for future work in Section 7.

2 Experimental system

The physical device being used in the work discussed here is shown in Fig. 1. The first two rectangular components form the body of the robot and are composed of an aluminum frame and a combination of aluminum and carbon fiber panels. The first compartment contains the microcontroller (Axiom PB-0555 microcontroller board with Motorola MPC555 PowerPC microprocessor), sensing devices, pectoral fin servo motors, and batteries. The second compartment contains the servo motors for the two tail links. The tail is composed of a wishbone shaped "peduncle" region and a rectangular flat plate for the caudal fin. The pectoral fins are actuated with Airtronics 94091Z super microlite servo motors, and the tail joints are actuated with Airtronics 94358Z ERG-VR high-torque micro servo motors. The pectoral fin motors are capable of 23 oz-in torque at 6V, and the tail servos are capable of 200 oz-in torque at 6V.

Figure 1: Side view of UW autonomous fin-articulated underwater robot.

All data collection, processing, and control function generation are handled internally through the microcontroller. The microcontroller has roughly 30 kB of memory which allows for the collection of about 45s of trajectory data (orientations, depth, time, servo commands). No external communication has been incorporated into this robot. Currently the robot has a 3D compass (Honeywell HMR3300) which can measure 360 degrees of yaw and ± 60 degrees for roll and pitch, and a pressure sensor (Druck PDCR4010) which can measure depth with a resolution of 0.08% of full scale (2.0atm for our device). To measure position in the plane perpendicular to gravity, an acoustic transducer system is currently in development.

Physical dimensions of the robot are shown in Fig. 2. The overall weight is approximately 2kg. The centers of buoyancy and gravity are engineered to be co-linear (but not coincident) along the body x_3 axis using externally applied styrofoam and steel shims for buoyancy and weight, respectively. The pectoral fins are composed of dense styrofoam and fiberglass and are located forward and above the center of mass. The fins are NACA 0021 airfoils with chord length $6.9cm$ and span $7.8cm$. The lift force generated by a fin is assumed to act at the quarter chord point of the fin. Given the aspect ratio and proximity to the body, are assumed to have lift coefficient $C_l(\alpha) = 0.07\alpha$ with angle of attack α measured in degrees.

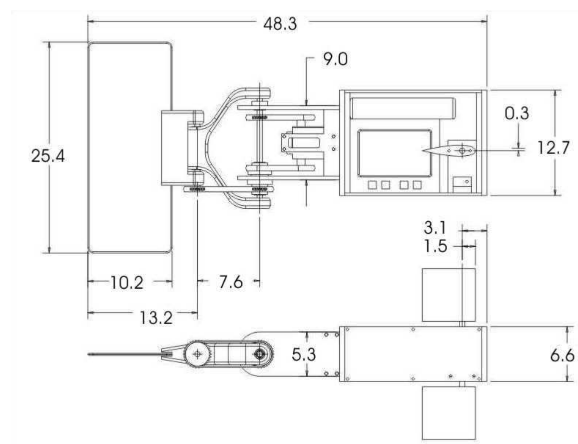

Figure 2: Physical dimensions of the fish robot (in cm).

3 Modeling

An idealized schematic of the system under consideration is shown in Fig. 3. Here we account for lift from the tail, L_t, drag from the body, D_b, lift and drag from the two pectoral fins, L_{p_r}, L_{p_l}, D_{p_r}, and D_{p_l}, the force of buoyancy, F_b, the force of gravity, F_g, and the moments resulting from these forces. We will approximate the body of the robot as an ellipsoid with major axis along the body longitude and minor axis along the body latitude.

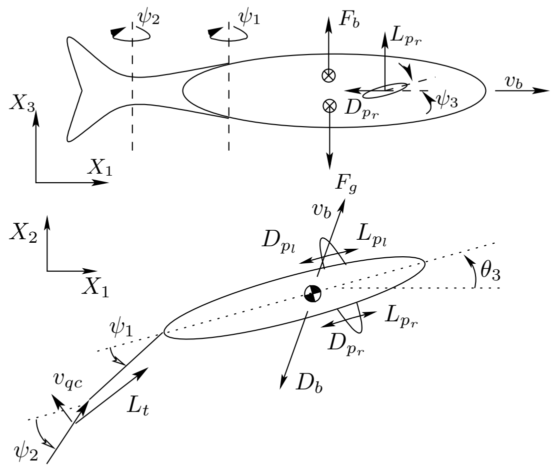

Figure 3: Conceptual design of fish robot.

3.1 Unforced equations of motion for body

The position and orientation of the body are denoted by g which can be written as

$$g = \begin{bmatrix} R & x \\ 0 & 1 \end{bmatrix}$$

where x is the position of the center of mass of the body relative to a fixed inertial reference frame measured relative to a body-fixed coordinate system. Here we take the longitudinal axis of the body to be the x_1 axis (positive forward), the lateral axis to be the x_2 axis (positive to the left), and the x_3 axis to be positive upward. The rotation matrix denotes the orientation of the body relative to the fixed body frame, and we will use ZYX Euler angles to determine this matrix from the body orientation vector θ in the analysis and simulations below. The translational and angular velocities are denoted by the vectors Ω and V. In this notation, the body velocity is then given by

$$\begin{aligned} \dot{R} &= R\widehat{\Omega} \\ \dot{x} &= RV \end{aligned} \tag{1}$$

where $\widehat{\Omega} = \begin{bmatrix} 0 & -\omega_3 & \omega_2 \\ \omega_3 & 0 & -\omega_1 \\ -\omega_2 & \omega_1 & 0 \end{bmatrix}$.

We assume that the fluid is incompressible, irrotational and inviscid. Using Kirchoff's equations [10], the unforced equations of motion may then be written as

$$\begin{aligned} \mathbf{J}\dot{\Omega} &= \mathbf{J}\Omega \times \Omega + \mathbf{M}V \times V \\ \mathbf{M}\dot{V} &= \mathbf{M}V \times \Omega \end{aligned}$$

where $\mathbf{J}$ and $\mathbf{M}$ are the inertia and mass matrices including added mass effects. Defining the system momentum, $p = [\Pi, P] = [\mathbf{J}\Omega, \mathbf{M}V]$, these equations can be expressed as

$$\dot{p} = \begin{bmatrix} \Pi \times \Omega + P \times V \\ P \times \Omega \end{bmatrix} \tag{2}$$

For an ellipsoid of mass m with body axes given by a_{x_1}, a_{x_2} and a_{x_3}, the added mass ([5]) in all three axes is $\frac{4}{3}\pi\rho a_{x_1} a_{x_2} a_{x_3}$. The moment of inertia about x_1 is $J_1 = \frac{1}{5}m(a_{x_2}^2 + a_{x_3}^2)$ with added inertia term $\frac{4}{15}\pi\rho a_{x_1} a_{x_2} a_{x_3}(a_{x_2}^2 + a_{x_3}^2)$ and similarly for the other two axes.

3.2 Potential forces

The vehicle is assumed to be neutrally buoyant with centers of buoyancy and gravity that are non-coincident but are co-located along an axis parallel to the body x_3 axis. The direction of gravity, in the body-fixed coordinate frame, is given by $\Gamma = R^T k$ where $k = [0,\ 0,\ -1]^T$. If the vector from the center of mass to the center of buoyancy is $r_b = [0,\ 0,\ h_b]^T$, then the effect of the non-coincident forces is a net torque $-\frac{1}{2}m\gamma\Gamma \times r_b$ where γ is the magnitude of the gravitational force.

3.3 Lift on airfoils

The actuation forces acting on the body are the thrust magnitude and orientation and the lift and drag from the two pectoral fins. Each of the fins may be allowed to pitch and heave with arbitrary frequency. As such we will use results from [19] to determine these forces. We refer the reader to that work for details, and simply state that if we neglect all shed vortices, then lift force on a pitching and heaving foil rotating with velocity ω_f about a point located at distance r_f from the quarter chord is given by

$$L_f = \frac{1}{2}\rho A_f C_l(\alpha)\widetilde{V}^2$$

where $\widetilde{V} = V_{f,qc} + r_f \times \omega_f$, and $V_{f,qc}$ is the velocity at the quarter chord point of the foil. We will assume a linear relation between lift coefficient and angle of attack. If we limit the angle of attack to ± 20 degrees, then we have $\sin(\alpha) \approx \alpha$ and can rewrite the lift equation as

$$L_f = \frac{1}{2}\rho A_f C_l(\widetilde{V} \times r_{le}) \times \widetilde{V}$$

where r_{le} is a unit vector pointing in the direction of the leading edge of the pectoral fin in body-frame coordinates.

Note that as we are assuming that the pectoral fins are parallel to the x_2 axis, $V_{f,qc} = [V_1,\ 0,\ V_3]$ for the pectoral fins, and the caudal fin is parallel to the z_3 axis so for the tail $V_{f,qc} = [V_1,\ V_2,\ 0]$.

3.4 Drag on airfoils

As the tail primarily functions in the wake of the body, we will assume that it generates negligible drag. For the body and pectoral fins, we will compute drag as

$$D_f = \frac{1}{2}\rho A_f C_d(\alpha)\widetilde{V}^2$$

where, as with lift, $\widetilde{V}$ takes into account velocity due to rotation. For the body, no effect will be felt from oscillation as the body is assumed to oscillate about its center of gravity and the body frame is located at the center of gravity. For the pectoral fins, $\widetilde{V} = V + r_f \times \omega_f$. This choice of drag is clearly a crude approximation and neglects the fact that the body is rotating as well as translating. As we will show, this assumption does not significantly affect our experimental results relative to the simulations.

3.5 Geometric mechanics

For systems such as this one where forces on the system are independent of the body position and orientation, we can apply geometric mechanics techniques in the form of a version of Hamel's equations to describe the system dynamics. We will simply state the resulting equations below and refer the reader to references (e.g. [1]) for full detail:

$$\begin{aligned} g^{-1}\dot{g} = \xi &= -\mathcal{A}(r)\dot{r} + \mathbb{I}(r)p \\ \dot{p} &= ad^*_\xi \frac{\partial \mathcal{L}}{\partial \xi} + F^{\mathcal{H}}_\xi(\xi, \dot{r}) + F_\xi \\ \mathcal{M}_{rr}(r)\ddot{r} &= \frac{\partial \mathcal{L}}{\partial r} + F_r \end{aligned} \tag{3}$$

where g are the position and orientation of the main body in a body-fixed coordinate frame, ξ is the main body velocity in body-fixed coordinates, r are the values of the joint (or "shape") states (here the pectoral joints and tail joints), $\mathcal{A}(r)$ is the local connection, $\mathbb{I}(r)$ is the locked inertia tensor, p is the bulk system momentum, $\mathcal{L}$ is the system Lagrangian, $F^{\mathcal{H}}_\xi$ are momenta terms that come from the presence of shape variations, F_ξ and F_r are external forces on the system, and $\mathcal{M}_{rr}$ is the kinetic energy metric for the shape states.

The first equation describes how to obtain the body motion from the momenta and shape, and for our system is just a re-expression of (1). The first term in the momentum equations is Kirchoff's equations for a solid body in a fluid (as given in (2)). The forces F_ξ are the potential forces, lift and drag as well as the moments induced by those forces. The final equation describes the fully controlled physical shape of the system which can be feedback linearized to make the r dynamics linear.

3.6 Simplified body orientation model

For the purposes of studying the use of actuated pectoral fin bowplanes for control, we will use a simplified model of the system. The thrust from the tail actuation will be treated as a force with actuated magnitude and orientation which are determined by the time average of the flapping motion of the tail. This approximation is reasonable as long as the tail oscillation frequency is at least an order of magnitude larger than the natural time constants of the unforced system. From prior work with a planar version of this system, we know that this assumption can be easily satisfied. Additionally, when the pectoral fins are not oscillating at a high frequency, but are simply being used for steering, we will neglect the effects of shape space dynamics in (3).

4 Accessibility and controllability

Given a system of the form $\dot{x} = f(x, u)$, the first question we should ask is whether the system has a controllable linearization either at a point or about a trajectory. While our system does not possess linear controllability at a point, work by other groups has shown that linearization about a trajectory can be achieved. We will take the alternate route of applying nonlinear control methods.

To begin, we will rewrite Eqs. (3) by defining $q = [p, r, \dot{r}]$ (note that g and ξ are completely determined by the variables forming q). The system equations may then be written as

$$\dot{q} = f_0(q) + \sum_{i=1}^{m} f_i(q)u_i(q,t)$$

where $q \in \mathbb{R}^{6+2m}$, $r, \dot{r} \in \mathbb{R}^m$, m is the number of control inputs, $f_0(q)$ is termed the system drift vector field, and $f_i(q)$ are termed the system control vector fields.

The Lie bracket of two vector fields f_i and f_j is denoted $[f_i, f_j]$ and is defined to be

$$[f_i, f_j] = \frac{\partial f_j}{\partial x} f_i - \frac{\partial f_i}{\partial x} f_j.$$

One can check that the Lie bracket satisfies the properties:

$$\begin{aligned} [f_i, f_i] &\equiv 0 \\ [f_i, f_j] &= -[f_j, f_i] \\ [f_i, [f_j, f_k]] &= -[f_j, [f_k, f_i]] - [f_k, [f_i, f_j]]. \end{aligned}$$

Lie brackets between control vector fields correspond to particular combinations of oscillatory, or area generating, motions of the corresponding control input functions. These vector fields then determine what system motion will be accomplished if the corresponding control input functions are applied to the system. An important point to note is that while those control inputs will generate the given motion along the vector field, they may also generate motion in other vector field directions.

Given a set $\mathcal{F}$ of C^∞ vector fields on a manifold M, the Lie algebra of $\mathcal{F}$, $L(\mathcal{F})$ is the set of all Lie brackets of elements of $\mathcal{F}$ and of all the Lie brackets of vector fields generated by Lie bracketing. The set $\mathcal{F}$ is said to satisfy the *accessibility property from a point* q_0 if, for every $T > 0$, the set of points reachable from q_0 in time $\leq T$ is nonempty. Effectively this just means that some motion can be achieved from point q_0. The family $\mathcal{F}$ satisfies the *Lie algebra rank condition(LARC) at a point* $q_0 \in M$ if the Lie algebra of $\mathcal{F}$ evaluated at q_0, $L(\mathcal{F})(q_0)$, is the whole tangent space of M at q_0. This statement means that the system could move in any direction from q_0, but not necessarily reach another point at a particular time or by following an arbitrary trajectory. If the LARC condition is satisfied, then the following will hold.

Proposition 4.1 ([20]) *Let $\mathcal{F}$ be a family of C^∞ vector fields on a C^∞ manifold M. Then the* LARC *at q_0 implies accessibility from q_0.*

However, this condition is fairly restrictive, and accessibility may be possible even if the condition is not met. If the Lie algebra evaluated at q_0 spans a subspace of the tangent space, then the system has accessibility restricted to the corresponding submanifold of M. Ideally, we would like to find vector fields that correspond to a particular direction when evaluated at any point in the state space. To determine these accessible directions for the robot, we will consider separately the cases of planar locomotion, and free body motion with the simplified thrust model.

4.1 Planar locomotion

From the earlier definitions, note that respectively f_1, f_2, f_3, and f_4 respectively correspond to the peduncle joint in the tail, the caudal joint in the tail, the right pectoral fin and the left pectoral fin. Determining the motions to which vector fields correspond in a system with this level of complexity is generally quite difficult. However, as the vector fields are analytic, one can evaluate them for Representative physical parameters and analyze the result for particular operating conditions. Straightforward, but involved, calculations have then shown in previous work [15] the following correspondence between vector fields and directions:

$$\begin{array}{rcl} \dot{\psi}_1 & \rightarrow & f_1 \\ \dot{\psi}_2 & \rightarrow & f_2 \\ \dot{x_1} & \rightarrow & [[f_0, f_1], [f_0, f_2]] \\ \dot{\theta}_3 & \rightarrow & [f_1, [f_0, [f_1, [f_0, f_2]]]] \end{array}$$

From this correspondence we can determine how to generate motion in the x_1 and θ_3 directions. Motion in the x_2 direction is coupled with the θ_3 direction, and an additional spanning vector field has not been found. However, as motion planning in the plane can be accomplished as long as a vehicle can move forward and turn with a finite radius, the robot can move between any two points with arbitrary initial and final orientation. The lack of the final vector field simply precludes such motions happening in arbitrary time scales.

4.2 Free body motion

To evaluate the additional motions that can be generated by oscillating the pectoral fins we will consider only the vector fields that correspond to the two fins. In this case, again evaluating the vector field parameters at representative values used in the simulations below, and using $\mathbf{e}_i$ to denote a unit vector in the ith direction (recall that the states are ordered according to $q = [p, r, \dot{r}]$), we have the following:

$$\begin{aligned} &[f_3, [f_0, f_3]] = \\ &\quad \left(3.5e^{-4}\cos^2(\psi_3)\sin(\psi_3) + 3.5e^{-4}\sin^3(\psi_3)\right)\mathbf{e}_1 \\ &\quad - \left(3.1e^{-5}\cos(\psi_3) + 3.1e^{-5}\sin(\psi_3)\right)\mathbf{e}_2 \\ &\quad +1.1e^{-4}\cos(\psi_3)\mathbf{e}_3 - 8e^{-6}\cos(\psi_4)\mathbf{e}_4 \\ &\quad - \left(8.6e^{-6}\cos^2(\psi_3)\sin(\psi_3) - 8.6e^{-6}\sin^3(\psi_3)\right)\mathbf{e}_6 \end{aligned}$$

$$\begin{aligned} &[f_4, [f_0, f_4]] = \\ &\quad - \left(3.5e^{-4}\cos^2(\psi_4)\sin(\psi_4) + 3.5e^{-4}\sin^3(\psi_4)\right)\mathbf{e}_1 \\ &\quad - \left(3.1e^{-5}\cos(\psi_4) + 3.1e^{-5}\sin(\psi_4)\right)\mathbf{e}_2 \\ &\quad -1.1e^{-4}\cos(\psi_4)\mathbf{e}_3 - 8e^{-6}\cos(\psi_4)\mathbf{e}_4 \\ &\quad - \left(8.6e^{-6}\cos^2(\psi_4)\sin(\psi_4) - 8.6e^{-6}\sin^3(\psi_4)\right)\mathbf{e}_6 \end{aligned}$$

$$\begin{aligned} &\left[[f_3, f_0], [f_4, f_0]\right] = \\ &\qquad \alpha_1\mathbf{e}_1 + \alpha_2\mathbf{e}_2 + \alpha_3\mathbf{e}_3 + \alpha_4\mathbf{e}_4 + \alpha_6\mathbf{e}_6 \end{aligned}$$

Considering the first of these combinations, and noting that the two joints are oscillating, we see that the roll and pitch will vary between two bounds while the yaw will steadily increase. Similarly for the second bracket combination, but the yaw will be in the opposite direction. With respect to the velocities of the first bracket combination, the vehicle will always have a positive forward motion and an oscillating depth. Again, the second bracket combination has the same velocities and neither vector field has a lateral velocity. For both of these choices then, we will get a forward gait.

In this last vector field, the term had to also be evaluated for typical state combinations due to its complexity. The dominant turning value is ω_3 and the dominant velocity is v_1 (about twice v_3). So here again we expect to get a forward gait, with a yaw.

5 Nonlinear control

For the class of nonlinear systems to which this one belongs, the use of superimposed periodic inputs with particular frequency relations has been shown to generate motion in desired directions that cannot be directly actuated. A particular set of oscillatory signals applied to the actuators of a system which results in a characteristic (stable) system response is generally referred to as a "gait". One method to construct gaits and produce motion in desired directions is to use a knowledge of the system Lie algebra, discussed in the previous section, and an application of averaging theory. To clarify these ideas, this section is organized as follows. A discussion of the relevant results from averaging theory will be presented. Full details of this work may be found in [23, 22]. Application of these ideas can be organized into construction of gaits for three classes of motions: (1) coordinated, oscillatory actuation of the tail with nonoscillatory actuation of the pectoral fins; (2) coordinated, oscillatory actuation of the pectoral fins with nonoscillatory actuation of the tail; (3) coordinated, oscillatory actuation of both the pectoral fins and of the tail. We will focus here on the first two classes and finish with a discussion of the use of feedback with these control inputs.

The simulation results demonstrating the different gaits are generated from two models. The model used for planar motion with tail oscillation comes from [16] and uses the physical parameters of that system. The simulations for the simplified body orientation model use $m = 2kg$, $h_b = 0.02$, $a_{x_1} = 0.15m$, $a_{x_2} = 0.05m$, $a_{x_3} = 0.075$.

5.1 Motion generation

Assume that each of the control functions u_i has been chosen to be of the form $u_i(q,t) = u_{i0}(q) + \sum_{j=1}^{N_j} u_{ij}(q)\sin(\frac{2\pi}{T}\omega_{ij}t + \phi_{ij})$ where $\omega_{ij} \in \mathbb{Z}$ and u_i is then the sum of a purely state dependent term and T-periodic functions. We may then rewrite the system as

$$\dot{q} = \tilde{f}(q) + \sum_{i=1}^{m} g_i(q,t) \tag{4}$$

where

$$\begin{aligned} \tilde{f}(q) &= f_0(q) + \sum_{i=1}^{m} f_i(q)u_{i0}(q) \\ g_i(q,t) &= \sum_{ij} f_i(q)u_{ij}(q)\sin(\frac{2\pi}{T}\omega_{ij}t + \phi_{ij}) \end{aligned}$$

and the g_i are thus T-periodic. We will additionally assume that T is small and that the functions $u_i(t)$ satisfy

$$\int_0^T (u_i(s_1) - u_{i0})ds = 0$$
$$\int_0^T \int_0^{s_2} (u_i(s_1) - u_{i0})ds_1 ds_2 = 0.$$

We then have the following results.

Lemma 5.1 ([22]) *Motion in the direction $[f_i, [f_0, f_j]]$ can be generated with control functions of the form*

$$\begin{aligned} u_i(q,t) &= u_{i0}(q) + u_{i1}(q)\sin(\frac{2\pi}{T}\omega t) \\ u_j(q,t) &= u_{j0}(q) + \sin(\frac{2\pi}{T}\omega t) \end{aligned}$$

or with

$$\begin{aligned} u_i(q,t) &= u_{i0}(q) + u_{i1}(q)\cos(\frac{2\pi}{T}\omega t) \\ u_j(q,t) &= u_{j0}(q) + \cos(\frac{2\pi}{T}\omega t) \end{aligned}$$

If $i = j$, use the definition for u_i.

Note that if $i = j$ above, only positive motions will be possible and the gait cannot be reversed.

Lemma 5.2 ([22]) *Motion in the direction $[[f_i, f_0], [f_j, f_0]]$ can be generated with control functions of the form*

$$\begin{aligned} u_i(q,t) &= u_{i0}(q) + u_{i1}(q)\cos(\frac{2\pi}{T}\omega t) \\ u_j(q,t) &= u_{j0}(q) + \sin(\frac{2\pi}{T}\omega t) \end{aligned}$$

Lemma 5.3 ([22]) *Define the following*

$$\chi_\alpha = \cos(\frac{2\pi}{T}\alpha\omega t)$$

Motion in the direction $[f_i, [f_0, [f_j, [f_0, f_k]]]]$ can be generated with control functions determined by the following three cases.

(a) $i = j = k$*:*

$$u_i(q,t) = u_{i0}(q) + u_{i1}(q)\chi_1$$

(b) $i = j$ *or* $i = k$ *or* $j = k$*: Assume* $i = j$ *and make similar choices in the other two cases.*

$$u_i(q,t) = u_{i0}(q) + \chi_1$$
$$u_k(q,t) = u_{k0}(q) + u_{k1}(q)\chi_2$$

(c) $i \neq j \neq k$*:*

$$u_i(q,t) = u_{i0}(q) + u_{i1}(q)\chi_3$$
$$u_j(q,t) = u_{j0}(q) + \chi_2$$
$$u_k(q,t) = u_{k0}(q) + \chi_1$$

5.2 Oscillatory caudal fin, nonoscillatory pectoral fins

Prior work with the planar version of this system demonstrated that a forward gait can be constructed by applying a sine to one tail joint and a cosine to the other, both at the same frequency. Turns can be generated in one of two ways. The first is to use the tail as a rudder by biasing the forward gait motions away from the main body line. The second, predicted by the geometric structure of the system equations, results by applying a cosine of one frequency to the first joint and a cosine of half that frequency to the second joint. These gaits can also be realized in the free-swimming robot with its caudal and pectoral fins.

Forward carangiform locomotion

As shown in Section 5, forward motion from oscillation of the tail can be achieved by inducing motion in the Lie bracket direction $[f_1, [f_0, f_2]]$. Using the results above, we see that this direction can be generated by the controls

$$u_1 = u_{11}\sin(\frac{2\pi}{T}\omega t),\ u_2 = u_{21}\cos(\frac{2\pi}{T}\omega t)$$

Applying these controls to the simulation of the planar version of this system discussed in [15, 16] gives the result shown in Fig. 4. In this case, we have chosen $u_{11} = 0.4$, $u_{21} = 0.4$, $\frac{2\pi}{T}\omega = 8$. Clearly the robot settles into a forward gait with a body motion that oscillates at the same frequency as the tail sweep.

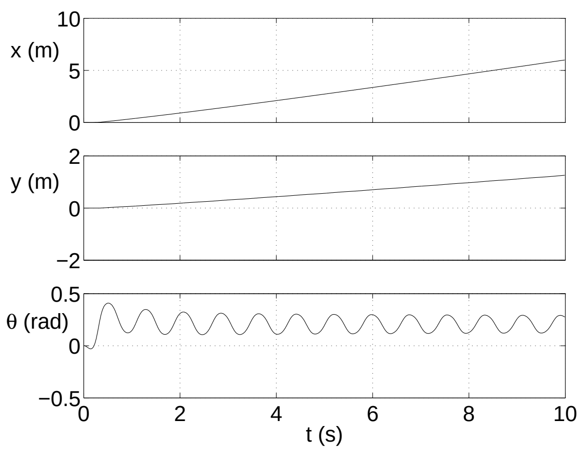

Figure 4: Simulation of carangiform forward locomotion [16].

Yaw actuation

The vector field $[f_1, [f_0, [f_1, [f_0, f_2]]]]$ has been shown to generate motion in the yaw direction of the vehicle using motion of the tail. This motion is higher order and therefore smaller in resulting body amplitude for similar tail motions than a vector field direction composed of fewer Lie brackets. As such, we do not expect that it would be implemented by a biological system, but it is of interest from a theoretical point of view. Control functions that will generate this motion are predicted from above to be

$$u_1 = u_{11}\cos(\frac{2\pi}{T}\omega t),\ u_2 = u_{21}\cos(\frac{4\pi}{T}\omega t).$$

Applying these controls to the simulation of the planar version of this system in [15, 16] gives the result shown in Fig. 5. For this case, we have chosen $u_{11} = 0.4$, $u_{21} = 0.4$, $\frac{2\pi}{T}\omega = 3.5$. Here we can see a clear turn about the x_3 axis with a small drift in the body position.

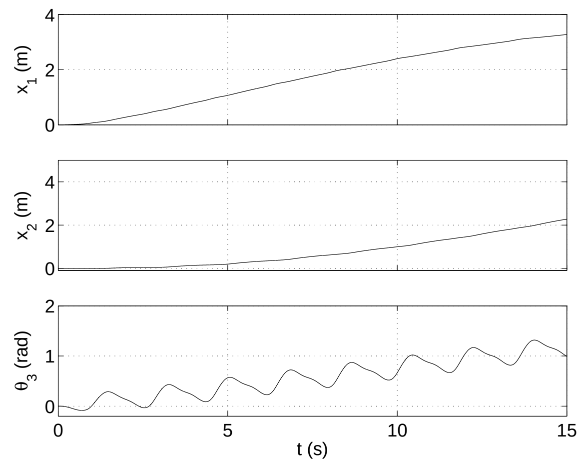

Figure 5: Simulation of carangiform turn [15]

Pitch and roll actuation

To generate the motions for pitch and roll using nonoscillatory motions for the pectoral fins and oscillatory actuation of the tail, we can use the simplified body orientation model from Section 3.6. In this system, pitch and roll are respectively achieved when a constant thrust is generated by the tail and the pectoral fins are either given identical orientations (pitch) or opposite orientations (roll). Simulations of the simplified body orientation model with the fins pitched up and then pitched oppositely are shown respectively in Figs. 6 and 7. A constraint thrust of 1N is used in both examples with fin angles of $0.1rad$. The effect of lift is clear in the diagrams as the system pitches downward.

5.3 Oscillatory pectoral fins, nonoscillatory caudal fin

We will now consider the effect of using the tail in a non-oscillatory mode so that it behaves as a rudder

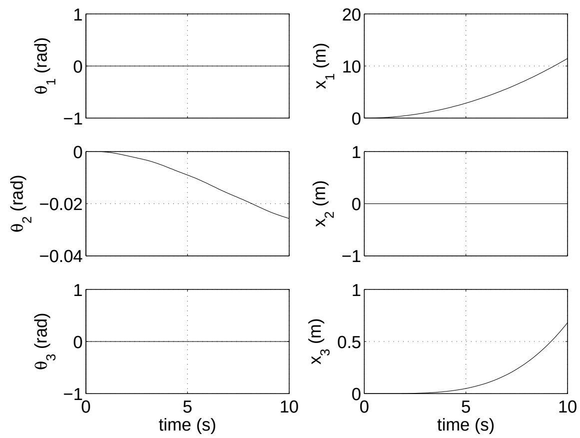

Figure 6: Simulation of pitch turning: $u_3 = u_4 = 0.2rad$.

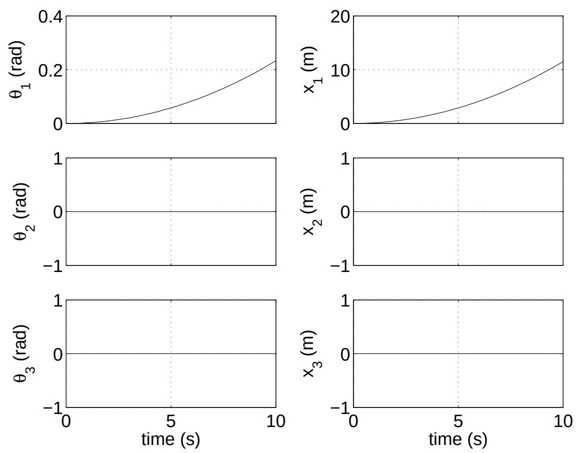

Figure 7: Simulation of roll turning: $u_3 = -u_4 = 0.2rad$.

rather than a propulsive mechanism. The first two gaits correspond to producing forward motion using oscillatory actuation of the two pectoral fins. the third gait will generate forward motion as well as a net yaw. Given the small size of these fins compared to the caudal fin as well as the numerical entries in the Lie algebra vector fields, we do not expect the motions to be large. However, for the purposes of small scale maneuvering, such gaits may have importance in engineered systems.

Forward dolphin locomotion

The vector fields $[f_3, [f_0, f_3]]$ and $[f_4, [f_0, f_4]]$ have equal forward motion and opposite yaw motion for identical input parameters. To generate this motion, we can apply control inputs

$$u_3 = u_{31} \sin(\frac{2\pi}{T}\omega t), \quad u_4 = u_{41} \sin(\frac{2\pi}{T}\omega t).$$

Choosing $u_{31} = u_{41} = 0.1rad$ and $\frac{2\pi}{T}\omega = 10$ gives the result shown in Fig. 8. The expected forward motion is

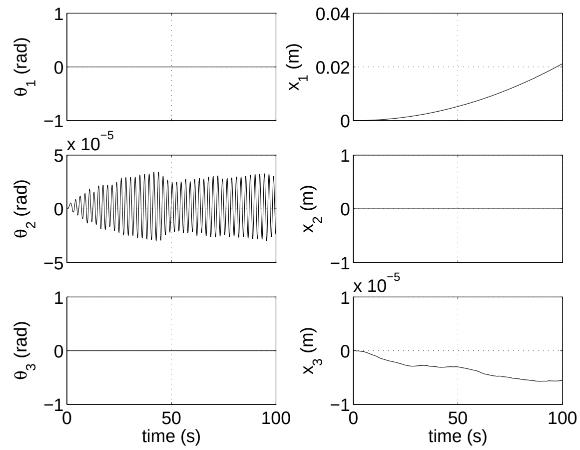

Figure 8: Forward locomotion from oscillatory dolphin motion of pectoral fins.

achieved as well as the net zero orientation change. Note that we could also use either fin individually or both with different magnitudes and frequencies and get a forward motion, but there would be a net orientation change. One can use this effect to produce desired turning.

Forward kicking locomotion

The controls in the previous case are also valid for generating forward motion with no net turn if we choose opposite amplitudes with identical magnitude and identical frequency. The result is a kicking type of motion as shown in Fig. 9. The results here are not quite as clean,

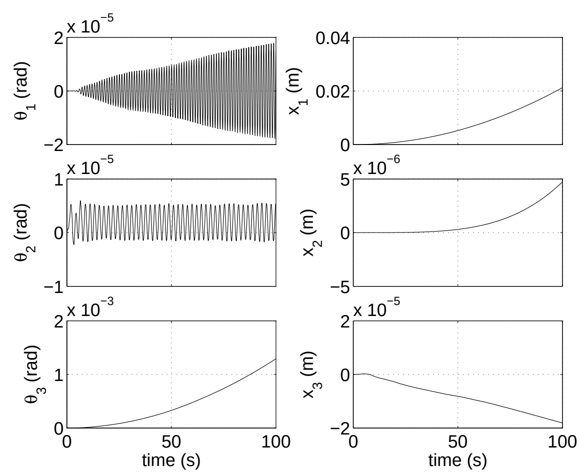

Figure 9: Forward locomotion from oscillatory kicking motion of pectoral fins.

but still demonstrate the expected behavior.

Yaw control

The vector field $[[f_3, f_0], [f_4, f_0]]$ will generate both a forward motion and a net yaw. This effect is predicted with the controls

$$u_3 = u_{31} \sin(\frac{2\pi}{T}\omega t), \quad u_4 = u_{41} \cos(\frac{2\pi}{T}\omega t)$$

and is shown in Fig. 10. As predicted, both a yaw and

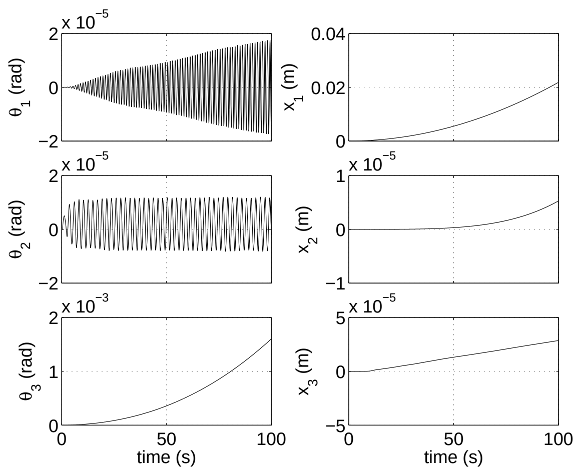

Figure 10: Forward turning motion from oscillating pectoral fins.

forward motion are generated.

Superimposed and higher order effects

Clearly one can continue to compute Lie brackets ad infinitum and determine control inputs to generate the corresponding motions. Further computations will not be made here, but some observations will be given. Each of the oscillatory motions constructed above was made to generate a single Lie bracket vector field direction. A natural question that arises is what can be achieved by superimposing the oscillatory and nonoscillatory inputs. As can be seen from the vector fields, inputs to generate forward and pitch or roll control could be constructed using the kicking or dolphin gate with a bias on the pectoral fins. In general if we can find a set of inputs that span the entire space, namely a set of linearly independent Lie bracket vector fields, we can potentially construct combinations that will give each of the individual motions. This task is clearly quite complicated, and as of yet, no method exists for determining either necessary or sufficient conditions on the system vector fields that hold in generality.

6 Experimental results

In the following, we will show some of the experimental results generated using the types of controls discussed earlier. The particular set of trajectories shown is limited to what can be measured using the on-board sensors, and therefore no planar position data is available.

6.1 Motion generation

Oscillatory caudal fin yaw gait

To demonstrate this gait, the controls (in degrees)

$$u_1 = 48\cos(5t), \quad u_2 = 48\cos(10t)$$

were applied to the robot with the result shown in Fig. 11. In comparison to the simulated system, we see that

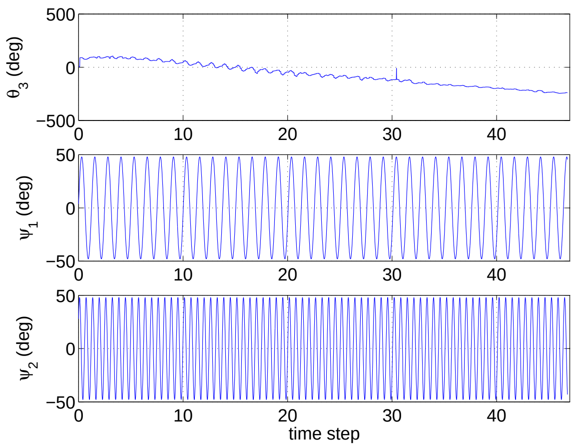

Figure 11: Oscillatory caudal fin yaw gait.

the robot demonstrates a much larger turning rate. However, the qualitative result is quite similar. Also, while this motion produces a definite turn in the yaw direction, it is not a motion one would generally associate with biological swimming. Also, the turn from this gait is much slower than what can be produced by biasing the tail when there is sufficient forward velocity, which makes the tail bias a preferable option for evading predators or capturing prey.

Oscillatory pectoral fin dolphin and kicking gaits

Both of these gaits were tested on the robot with inputs of the form

$$u_3 = 10\sin(12t), \quad u_4 = \pm 10\sin(12t)$$

While we are unable to collect the planar position data for this experiment, video is available at *http://vger.aa.washington.edu*. In both cases the robot moved approximately 1m in 20sec which is much larger than what was predicted in the simulation. Clearly the simulation is a crude approximation of this robot and would benefit from refinement.

6.2 Trajectory tracking

The primary effect of the unaveraged motion is to superimpose a higher frequency body oscillation over the natural oscillation of the body. This effect will mean that when developing our feedback controllers, we will need to compute the feedback error as an average over the tail oscillation period, but otherwise may proceed as if the oscillation were not present (for further mathematical details on this topic see [23]).

As has been demonstrated in earlier work with the planar system [16] and in the mathematical development [23, 22], by evaluating the actual and desired system configurations and velocities after each oscillatory cycle, an error function can be generated and used to modify the cyclic actuation of the system. the feedback terms are only updated after whole cycles of oscillation in order to average out the naturally induced oscillation in the body from the underlying gross system motion. For the full mathematical details, we refer the reader to [22].

Heading control

To implement heading control, we will apply a basic tail oscillation and bias the tail as a rudder to produce turning. The controls then have the form

$$u_1 = \alpha_1 \sin(\omega t) + \gamma, \quad u_2 = \alpha_2 \cos(\omega t) + \gamma$$
$$u_1 = u_2 = -k_p e - k_d \dot{e} - k_i \int e$$

where $\gamma = -k_p e - k_d \dot{e} - k_i \int e$ and $e = \theta_{3d} - \theta_3$. Figure 13 shows data for the use of these control functions with tail joint amplitudes $\alpha_1 = 24deg$, $\alpha_2 = 36deg$, $\omega = 14rad/s$, $k_p = 0.32$ degree bias per degrees error, $k_d = 0.08$ degrees bias per deg/s error, and $k_i = 0$. The

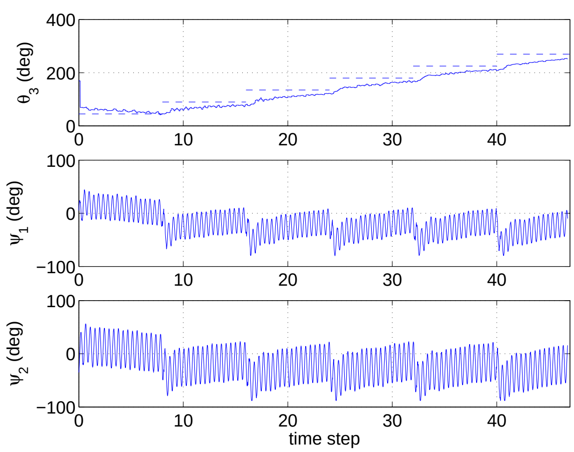

Figure 12: Heading control with oscillatory tail actuation.

dashed lines represent the target angle, which changes over time. As we see, the robot gets fairly close to the desired angles, but appears to be demonstrating overdamped behavior and would probably benefit from the use of integral control.

Depth control

As we have seen from the simplified body model, depth control can be achieved if we have forward velocity from the tail and use the pectoral fins to generate positive and negative lift. Superimposing the controls for tail thrust generation and pectoral fin lift generation, we have the control functions

$$u_1 = \alpha_1 \sin(\omega t), \quad u_2 = \alpha_2 \cos(\omega t)$$
$$u_3 = u_4 = -k_p e - k_d \dot{e} - k_i \int e$$

where $e = x_{3d} - x_3$. Figure 13 shows data for the use of these control functions with tail joint amplitudes $\alpha_1 = 24deg$, $\alpha_2 = 36deg$, $\omega = 14$, $k_p = 78.7deg/m$, $k_d = 7.87deg/m/s$, and $k_i = 7.87deg/m \cdot s$. The pectoral fin joints are limited to a maximum pitch of 40deg, and the integral term is limited to a maximum value of 0.15ms to prevent windup effects. The robot was started at the

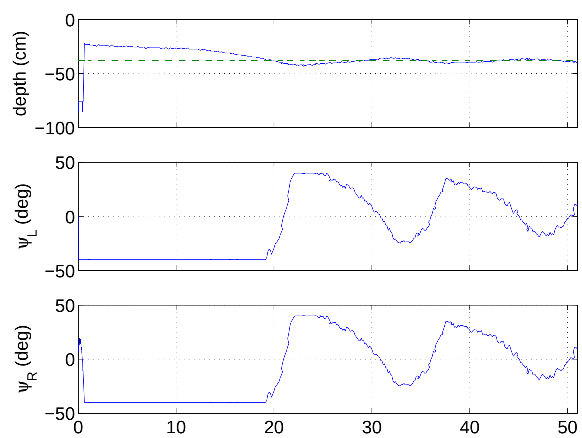

Figure 13: Depth control with oscillatory tail and pectoral fin actuation.

surface and given a target depth of 38cm. As we can see, the pectoral fins initially set to their maximum value to produce as much motion downwards as possible. The fins then quickly drove the error to within 2cm of the desired value of 38cm below the surface of the water.

7 Conclusions and future work

In this work, we have shown how the techniques of geometric modeling and nonlinear control theory can be applied to the task of control construction for a swimming robot. While the model being used is quite crude, clearly it is sufficient as a design tool in these initial studies. A more accurate model would, of course, lead to greater efficiency and better response in the system. Future work in this area is directed at models that include more complex fluid effects and which can include flexible foils with controlled shape. Investigations into optimal control selection for gait construction is also in progress.

The robot being used here is novel in that it controls both forward propulsion and depth with fins. These actuation surfaces are clearly sufficient for the tasks which have been demonstrated here. Ongoing work is addressing the construction of more agile maneuvering, and improved performance at low speeds. Most likely, deformable fins will be an important component of reaching this goal. More immediately, the next version of this robot will have a more ellipsoid body as well as actuation to maintain neutral buoyancy at all depths. Clearly this buoyancy control may also be used as a means of actuation although its purpose in future work will be to prevent effects of weight and buoyancy from interfering with the control methodologies in development.

References

[1] J.E. Marsden A.M. Bloch, P.S. Krishnaprasad and R.M. Murray. Nonholonomic mechanical systems with symmetry. *Arch. Rational Mech. Anal*, 136:21–99, 1996.

[2] J. M. Anderson and P. A. Kerrebrack. The vorticity control unmanned undersea vehicle–an autonomous vehicle employing fi sh swimming propulsion and maneuvering. In *Proc. 10th Int. Sym. Unmanned Untethered Submersible Tech.*, pages 189–95, Durham, NH, Sep. 1997.

[3] D. Barrett, M. Grosenbaugh, and M. S. Triantafyllou. The optimal control of a fexible hull robotic undersea vehicle propelled by an oscillating foil. In *Proc. 1996 Symp. Aut. Underwater Veh. Tech.*, pages 1–9, 1996.

[4] P. Bhatta and N. E. Leonard. Stabilization and coordination of underwater gliders. In *Proc. 41st IEEE Conf. Dec. Cont.*, pages 2081–2086, 2002.

[5] C. E. Brennen. A review of added mass and fluid inertial forces. Technical Report CR82.010, Naval Civil Engineering Laboratory, Port Hueneme, CA, Jan. 1982.

[6] S. Childress. *Mechanics of Swimming and Flying*. Cambridge University Press, Cambridge, 1981.

[7] N. Kato and T. Inaba. Guidance and control of fi sh robot with apparatus of pectoral fi n motion. In *Proc. 1998 IEEE Int. Conf. Rob. Aut.*, pages 446–51, 1998.

[8] S. D. Kelly, R. J. Mason, C. T. Anhalt, R. M. Murray, and J. W. Burdick. Modelling and experimental investigation of carangiform locomotion for control. In *Proc. Amer. Contr. Conf.*, pages 1271–6, 1998.

[9] S. D. Kelly and R. M. Murray. Modelling effi cient pisciform swimming for control. *Int. J. Rob. Nonlinear Contr.*, 10(4):217–41, 2000.

[10] H. Lamb. *Hydrodynamics*. Dover Publications, New York, NY, 6th edition, 1932.

[11] P. Y. Li and S. Saimek. Modeling and estimation of hydrodynamic potentials. In *Proc. 38th IEEE Conf. Dec. Cont.*, pages 3253–8, 1999.

[12] J. L. Lighthill. *Mathematical Biofluiddynamics*. SIAM, Philadelphia, 1975.

[13] R. J. Mason and J. W. Burdick. Construction and modelling of a carangiform robotic fi sh. In *Proc. 1999 Int. Symp. Exp. Rob.*, pages 235–42, 1999.

[14] R. J. Mason and J. W. Burdick. Experiments in carangiform robotic fi sh locomotion. In *Proc. IEEE Int. Conf. Rob. Aut.*, pages 428–35, 2000.

[15] K. A. Morgansen, V. Duindam, R. J. Mason, J. W. Burdick, and R. M. Murray. Nonlinear control methods for planar carangiform robot fi sh locomotion. In *Proc. IEEE Int. Conf. Rob. Aut.*, pages 427–34, 2001.

[16] K. A. Morgansen, P. A. Vela, and J. W. Burdick. Trajectory stabilization for a planar carangiform robot fi sh. In *Proc. IEEE Int. Conf. Rob. Aut.*, pages 756–762, 2002.

[17] J. N. Newman and T. Y. Wu. Hydrodynamical aspects of fi sh swimming. In T. Wu, C. Brokaw, and C. Brennen, editors, *Swimming and Flying in Nature, Vol 2.*, pages 615–34. Plenum Press, New York, 1975.

[18] S. Saimek and P. Y. Li. Motion planning and control of a swimming machine. In *Proc. Amer. Contr. Conf.*, pages 125–30, 2001.

[19] K. Streitlien and M. S. Triantafyllou. Force and moment on a joukowski profi le in the presence of point vortices. *AIAA J.*, 33(4):603–610, Apr. 1995.

[20] H.J. Sussmann and J. Jurdjevic. Controllability of nonlinear systems. *J. Differential Equations*, 12(1):95–116, Jul. 1972.

[21] M. S. Triantafyllou and G.S . Triantafyllou. An effi cient swimming machine. *Scientifi c American*, pages 64–70, Mar. 1995.

[22] P. A. Vela, K. A. Morgansen, and J. W. Burdick. Second order averaging methods and oscillatory feedback control of underactuated mechanical systems. *SIAM J. Contr. Optim.*, 2002. in preparation.

[23] P. A. Vela, K. A. Morgansen, and J. W. Burdick. Second order averaging methods for oscillatory control of underactuated mechanical systems. In *Proc. Amer. Contr. Conf.*, pages 4672–4677, 2002.

[24] M. J. Wolfgang, J. M. Anderson, M. A. Grosenbaugh, D. K. P. Yue, and M. S. Triantafyllou. Near-body fbw dynamics in swimming fi sh. *J. Exp. Biology*, 202(17):2303–7, 1999.

[25] C. A. Woolsey and N. E. Leonard. Underwater vehicle stabilization by internal rotors. In *Proc. Amer. Contr. Conf.*, pages 3417–21, 1999.